



# LUND UNIVERSITY

## Review of Wheel Modeling and Friction Estimation

Svendenius, Jacob; Wittenmark, Björn

2003

*Document Version:*

Publisher's PDF, also known as Version of record

[Link to publication](#)

*Citation for published version (APA):*

Svendenius, J., & Wittenmark, B. (2003). *Review of Wheel Modeling and Friction Estimation*. (Technical Reports TFRT-7607). Department of Automatic Control, Lund Institute of Technology (LTH).

*Total number of authors:*

2

### General rights

Unless other specific re-use rights are stated the following general rights apply:

Copyright and moral rights for the publications made accessible in the public portal are retained by the authors and/or other copyright owners and it is a condition of accessing publications that users recognise and abide by the legal requirements associated with these rights.

- Users may download and print one copy of any publication from the public portal for the purpose of private study or research.
- You may not further distribute the material or use it for any profit-making activity or commercial gain
- You may freely distribute the URL identifying the publication in the public portal

Read more about Creative commons licenses: <https://creativecommons.org/licenses/>

### Take down policy

If you believe that this document breaches copyright please contact us providing details, and we will remove access to the work immediately and investigate your claim.

LUND UNIVERSITY

PO Box 117  
221 00 Lund  
+46 46-222 00 00

ISSN 0280-5316  
ISRN LUTFD2/TFRT--7607--SE

# Review of Wheel Modeling and Friction Estimation

Jacob Svendenius  
Björn Wittenmark

Department of Automatic Control  
Lund Institute of Technology  
Augusti 2003

<b>Department of Automatic Control</b> <b>Lund Institute of Technology</b> <b>Box 118</b> <b>SE-221 00 Lund Sweden</b>	<i>Document name</i> INTERNAL REPORT	
	<i>Date of issue</i> August 2003	
	<i>Document Number</i> ISRN LUTFD2/TFRT--7607--SE	
<i>Author(s)</i> Jacob Svendenius	<i>Supervisor</i> Björn Wittenmark	
	<i>Sponsoring organisation</i> Haldex Brake Products AB	
<i>Title and subtitle</i> Review of Wheel Modeling and Friction Estimation		
<i>Abstract</i> <p>In this report research about tire modeling and friction estimation is collected and resumed. The report also covers the brush-model explanation to the slip phenomenon that comes up when the rim transmits a force to the ground through the tire when the wheel is rolling. The term <i>slip</i> significance the difference between the wheel velocity and the vehicle velocity when a driving or braking force is working on the tire. Most of the approaches that estimate tire friction build on the relation between the slip and the force that works on the tire. The paper also describes a couple of ways to include an extra calibration parameter in the brush model to improve its accuracy and enhance the friction estimation at low force excitations. Finally, results from simulation of friction estimation are presented.</p>		
<i>Key words</i> Tire Model, Brush Model, Slip, Friction Estimation		
<i>Classification system and/ or index terms (if any)</i>		
<i>Supplementary bibliographical information</i>		
<i>ISSN and key title</i> 0280-5316		<i>ISBN</i>
<i>Language</i> English	<i>Number of pages</i> 38	<i>Recipient's notes</i>
<i>Security classification</i>		

The report may be ordered from the Department of Automatic Control or borrowed through:  
University Library 2, Box 3, SE-221 00 Lund, Sweden  
Fax +46 46 222 44 22 E-mail ub2@ub2.lu.se

# Contents

<b>1. Introduction</b>	5
<b>2. Tire modeling</b>	5
2.1 Vertical deformation pressure distribution	5
2.2 Inputs and output for horizontal tire modeling	7
2.3 Brush model	9
2.4 Empirical models	14
<b>3. Estimation models</b>	16
3.1 Slip based friction estimation according to NIRA-dynamics	16
3.2 Brake force estimation with a Kalman-Busy Filter	17
3.3 GPS-based identification of the lateral tire-road friction coefficient	18
3.4 Optimal braking and friction estimation with the LuGre model	19
3.5 Extended Braking Stiffness (XBS)	19
3.6 Lateral friction estimation using the brush tire model	20
3.7 Longitudinal friction estimation using the brush tire model	20
3.8 Friction estimation for vehicle path prediction	21
3.9 Discussion	22
<b>4. Changes to the Brush Tire Model to Enhance Friction Estimation</b>	22
4.1 Pressure distribution	23
4.2 Velocity dependent friction	27
4.3 Taylor expansion	30
4.4 Velocity dependency	31
<b>5. Simulation of Friction Estimation with Brush Model</b>	32
5.1 Data generation	32
5.2 Estimation of brush model parameters	32
5.3 Estimation results	34
5.4 Effect of the calibrating $d$ -factor	35
<b>6. Conclusions</b>	36
<b>7. References</b>	38



## 1. Introduction

In this report research about tire modeling and friction estimation is collected and resumed. It also covers the brush-model explanation to the slip phenomenon that comes up when the rim transmits a force to the ground through the tire when the wheel is rolling. The term *slip* significance the difference between the wheel velocity and the vehicle velocity when a driving or braking force is working on the tire. Most of the approaches that estimate tire friction build on the relation between the slip and the force that works on the tire. The paper also describes a couple of ways to include an extra calibration parameter in the brush model to improve its accuracy and enhance the friction estimation at low excitations. Finally, results from simulation of friction estimation are presented.

The brush-model used for the estimation and empirical tire model are described in Section 2 The estimation review, Section 3, presents techniques developed by among others F. Gustafsson [6], L. Ray [16] and C. Canudas de Wit [4]. Section 4 contains an extension of the brush model and simulated estimation results are given in Section 5.

## 2. Tire modeling

The main purpose of a tire is to transmitt forces between the road and the rim so that the driver can control the vehicle. The tire also works as a low pass filter in the suspension system by reducing the high frequency vibrations from small unevennesses in the road. A lot of work has been done in the area of modeling tires and it covers everything from simple models aiming for understanding the physics to advanced finite-element models that can predict the behavior precisely. An exact analysis of the tire and its dynamical properties is very complex and is not realistic to implement in a vehicle system. Since the properties of different tires differ a lot the system has to know these properties when the tire is changed. The properties also change by wear, temperature, road conditions, etc. Therefore, researchers have developed empirical models including a few parameters, which can be determined by testing the tire. These models can then be used for calculations in simulations or real-time implementations. The possibility to use these models in a vehicle system is better, but still limited since factors from the driving environment affect the friction properties. The modeling in this paper will be very basic, with the aim to make the reader understand the physics behind the slip behavior of tires. The model is aimed to be general and the number of parameters is kept as low as possible.

### 2.1 Vertical deformation pressure distribution

Exposed to a vertical load the tire will deform. An exact analysis of the deformation requires good calculation tools and accurate information about the tire design and actual conditions, as axle load, road surface, and temperature. Schematicly, the deformation can be divided into two parts. One part from the change of the carcass shape and one from the compression of the rubber material. If the carcass deformation is moderate the air volume in the tire will remain nearly constant and no consideration to increased tire pressure is necessary. In the static case, i.e. when the wheel is not

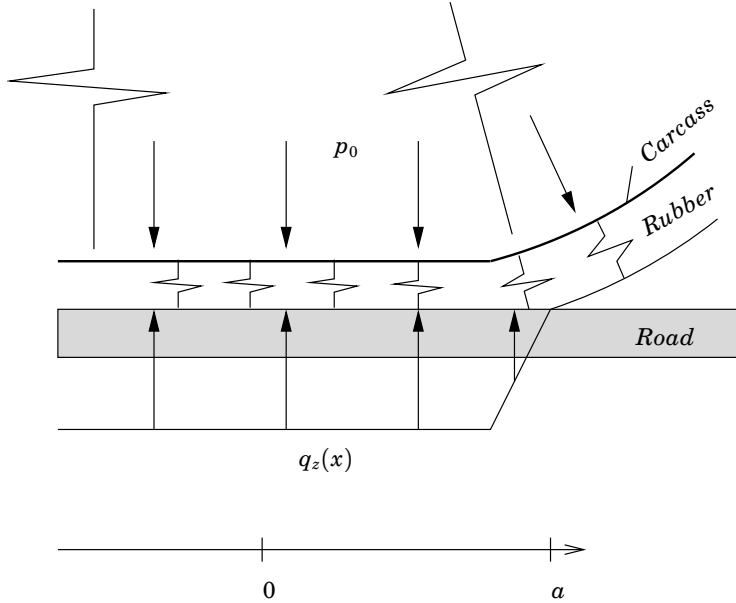


**Figure 1** Illustration of the vertical pressure distribution in a longitudinal cut of the tire. Note that  $q_z(x) = p_0$  in the major part of the cut.

rolling, the maximal pressure between the tire and the road, normally, can not exceed the pressure inside the tire,  $p_0$ . There is an area in the center of the contact patch where the pressure is equal to  $p_0$ . In the outer region where the carcass lifts from the ground the compression of the rubber gives a smooth transition of the pressure from  $p_0$  to 0, where the contact area ends. The pressure distribution in a longitudinal cut of the tire then might look as the example shown in Figure 1. In the lateral direction the distribution depends on shape of the carcass. An arched carcass, which corresponds to a well-inflated tire, gives a round contact patch. A poorly inflated tire results in a more flat carcass, which gives a more rectangular patch. In Figure 2 these two different special cases are shown and any intermediate solution is realistic. In the first case it is assumed that the contact zone has a shape of a circle or ellipse, with the area  $A = \pi ac$ . There is a linear relation between  $a$  and  $c$  and using  $F_z \approx p_0 A = k_0 a^2$  makes the contact length  $a$  proportional to  $\sqrt{F_z}$ . In the second case where  $A = 4ab$ ,  $a$  is instead linear to  $F_z$ . An example of the pressure distribution is shown to the left in Figure 3 for a non-rolling tire.

For the dynamic case it is different. The movement of the wheel changes the appearance of the pressure distribution and it will no longer be symmetric. When the wheel is rotating it deforms continuously and a braking torque called rolling resistance is developed. The pressure increases in the front half of the contact patch and decreases in the rear half. The amount of the change is depending on the velocity, the damping, and the mass of the deformed material.

How a braking/driving or cornering force changes the pressure distribution is not obvious. In general, the center for the vertical force moves in the opposite direction as the generated tire force is working [17].

When the pressure distribution is used further in the paper, it is laterally lumped, i.e. the lateral average is calculated. The pressure distribution

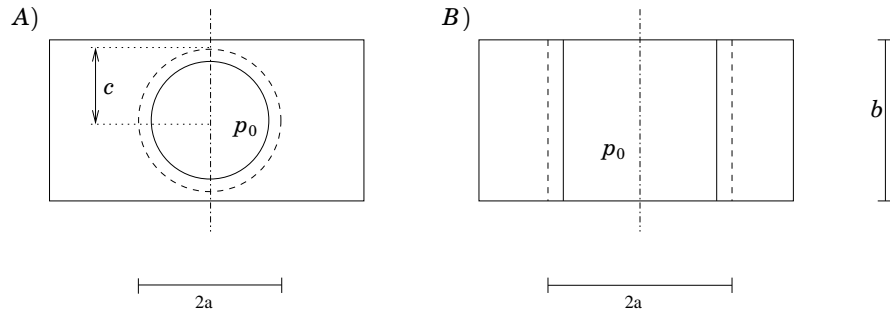


**Figure 2** Illustration of the tire contact patch (top view). Inside the solid lines the pressure is  $p_0$ , then it decreases to zero at the dashed line. A) Well-inflated tire; B) Poorly inflated tire.

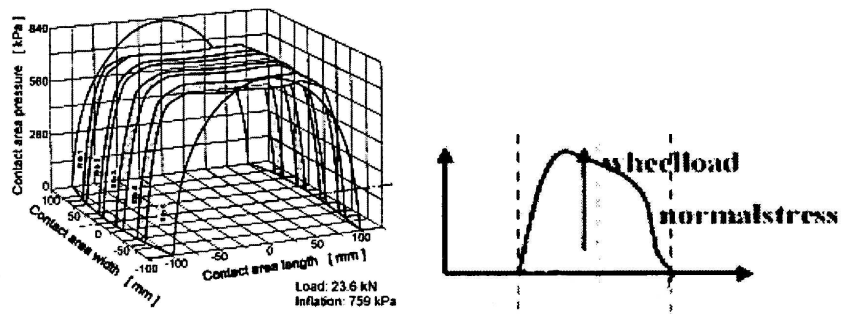


**Figure 3** Example of vertical pressure distribution. To the left it is shown for the whole contact patch of a non-rolling tire and to the right only the lateral average is shown for a rolling tire. Reprinted from [15].

in N/m is then given as a function of the longitudinal coordinate  $x$ . A common assumption is that the lumped pressure curve has a parabolic shape, with its peak at the center of the contact patch at standstill. For a rolling tire the peak moves forward and if the tire develops any force the peak moves as described above.

## 2.2 Inputs and output for horizontal tire modeling

It is difficult to understand how the tire develops a horizontal force if one do not know about the vehicle dynamics. As mentioned before a deformation of the tire is necessary to make it deliver a force. A deformation is achieved when the contact between the wheel and the road is forced to move in a different direction than the hub or when there is a torque working on the wheel preventing it from free rolling. If the driver turns the steering wheel, the front tires get another direction than the car and they will produce a force in the lateral direction, which affects the movement and makes the car turn. The necessary inputs from the vehicle model to tire model and its produced outputs are shown in Figure 4. The horizontal force from a tire use to be split in one lateral (indexed 'y' in the figure) and one longitudinal (indexed 'x') part, as shown in Figure 5. When there is a lateral force or when there are non-symmetric factors affecting the tire (uneven wear, for example) there also is a torque, in the literature called "self aligning torque". In Figure 5 the velocity vectors are the movements of the wheel



hub and the forces are working in the contact patch between tire and the road.

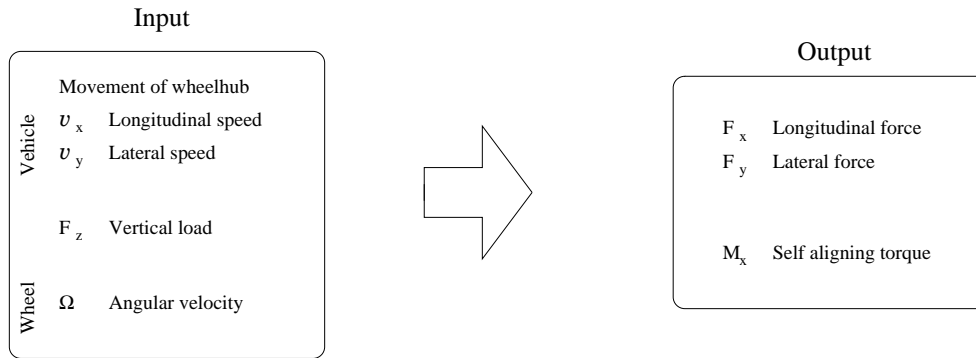


**Figure 4** Basic input-output signals for a tire model.

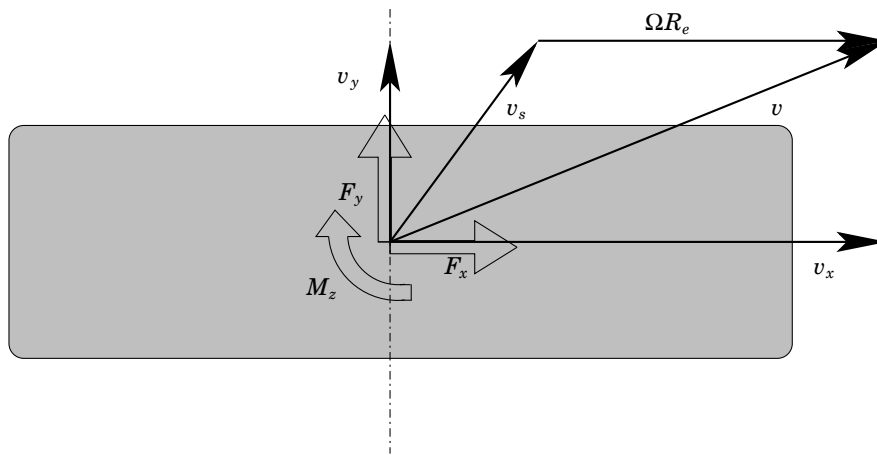


**Figure 5** Forces and movements in a tire model.  $R_e$  is the rolling radius of the tire.

**Slip Definitions** One of the mostly used terms in tire modeling is *slip*. It can be defined in a couple of ways and the difference between the definitions is how to normalize the slip velocity.

Origin	Notation	Long.	Lateral
SAE, ISO	$\kappa$	$v_{sx}/v_x$	$v_y/v_x$
Praxis	$s$	$v_{sx}/ \vec{v} $	$v_y/ \vec{v} $
Physical	$\sigma$	$v_{sx}/(\Omega R_e)$	$v_y/(\Omega R_e)$

**Table 1** Slip definitions. Note that  $v_{sx} = v_x - \Omega R_e$ , i.e. the longitudinal component of  $v_s$ .

The definition denoted  $s$  is the most convenient definition. It gets singular only at standstill of the vehicle and the value will always stay between  $-1$  and  $1$ , when braking or cornering (for driving often  $\sigma$  is used since it

always has proper values then). The other definitions ( $\kappa$ ,  $\sigma$ ) get singular either at wheel-lock or when the car only has lateral velocity. In Section 2.3 an expression depending on  $\sigma_x$  is derived. The slip denoted by  $\sigma$  corresponds to the deformation of the rubber in the tire contact patch.  $s$  and  $\kappa$  corresponds to the relative velocity between the tire and the road. For the empirical modeling the main thing may not be how to define the slip, but rather to know which definition that has been used for the measurements.

### 2.3 Brush model

In the brush model [13] it is assumed that the slip is caused by deformation of the rubber volume that is between the tire carcass and the ground. The volume is approximated as small brush elements, attached to the carcass, see Figure 6. The carcass is assumed to be stiff and it can neither stretch nor shrink, but it can still flex towards the hub. Every brush element can deform independently of the other.

A brush element  $i$  comes in contact with the road at time  $t=0$  and at the position  $x = a$ . The position of an element can be defined at its upper point ( $x_{ci}$ , attached to the carcass) or at its lower point ( $x_{ri}$ , the contact to the road), see Figure 7. As long as there is no sliding the positions will be

$$x_{ci} = a - \int_0^t \Omega R_e dt \quad (1)$$

$$x_{ri} = a - \int_0^t v_x dt \quad (2)$$

The deformation of the element is:

$$\delta_i = x_{ci} - x_{ri} = \int_0^t v_x - \Omega R_e dt = \int_0^t v_{sx} dt \quad (3)$$

If constant velocities are assumed, (3) together with (1) or (2) gives

$$\delta_i = \frac{v_{sx}}{\Omega R_e} (a - x_{ci}) = \frac{v_{sx}}{v_x} (a - x_{ri}) \quad (4)$$

where  $v_{sx}/(\Omega R_e)$  is the longitudinal slip denoted  $\sigma_x$ .

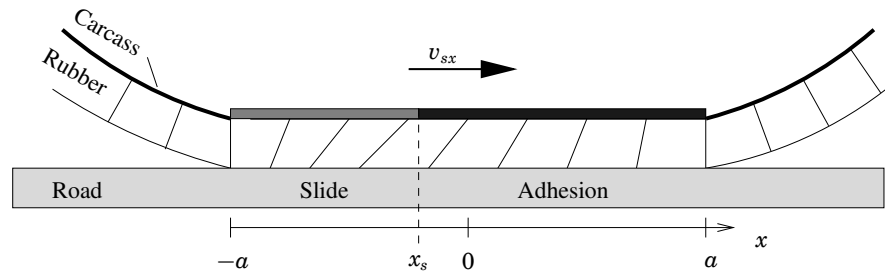


**Figure 6** Illustration showing the deformation of the rubber layer between the tire carcass and the road according to the brush model. The carcass moves with the velocity  $v_{sx}$  relative the road. The contact zone moves with the vehicle velocity  $v_x$ .

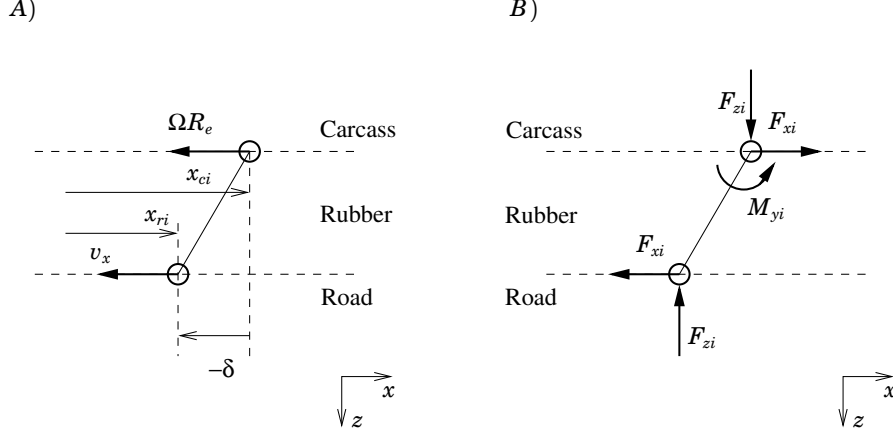


**Figure 7** A) The relative velocity and the position of upper and lower point of a brush element. B) The force equilibrium of the element. The additional torque  $M_{yi}$  working on the element to get rotational balance is not used in any calculations.

Rubber does not necessarily deform linearly, but it is approximated in that way. The force needed to achieve the amount of deformation given in (3) is then

$$F_{xi} = k\delta_i \quad (5)$$

The deformation of a bristle is limited by the friction between the tire and the road and the maximum force acting on the brush element is given by

$$F_{xi,max} = \mu F_{zi} \quad (6)$$

Putting (5) and (6) together the maximal deformation can be expressed as

$$\delta_{i,max} = \frac{\mu F_{zi}}{k} \quad (7)$$

The brush element starts to slide when the deformation reaches this value. The force acting on the bristle is then  $\mu F_{zi}$ . Three different choices for the entire contact patch arises.

- Adhesion in the entire contact area. The slip curve is only depending on the rubber properties.
- Both sliding and adhesion. The contact area is split into two sections, one with adhesion and one with sliding.
- The entire tire surface slides against the ground. The braking force is then only depending on the friction coefficient at the actual condition.

When both adhesion and sliding occurs in the contact patch it is possible to calculate the position where the sliding starts, the so called breakaway point. Use of (4) and (7) renders

$$x_{cis} = a - \frac{\mu F_{zi} \Omega R_e}{v_{sx} k} \quad (8)$$

The partition of the contact patch into discrete bristle elements is abandoned and an integration over the whole contact length is performed instead. The following changes,  $k = c_p dx_c$  and  $F_{zi} = q_z(x_c) dx_c$  are introduced, where  $c_p$  denotes stiffness per length unit and  $q_z$  is the vertical

force per length unit between tire and road. Adding the force from the area of adhesion to the force from the sliding region the total braking force is

$$F_x = \int_{x_{cs}}^a c_p \frac{v_{sx}}{\Omega R_e} (a - x_c) dx_c + \int_a^{x_{cs}} q_z(x_c) \mu dx_c \quad (9)$$

It can be discussed whether to use  $x_r$  or  $x_c$  in the the formulas. For the vertical force  $F_{zi} = q_z(x_{ci})$ ,  $x_r$  might be used instead of  $x_c$ , while the pressure distribution usually is defined between the tire and the road. However, since the bristles are attached to the carcass they are equally spaced there, i.e.  $dx_c$  is constant.  $dx_r$  is not constant along the contact length and then not suitable as integration variable. From now on the index  $c$  is dropped and  $x$  denotes the carcass position of the bristle. The vertical pressure

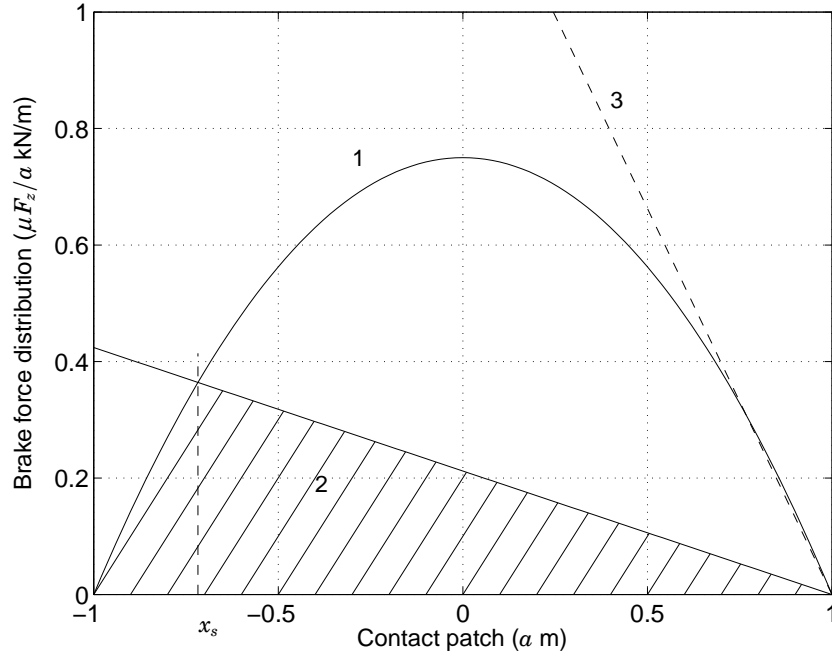


**Figure 8** The deformation of the rubber layer between carcass and road. Curve 1: Maximum available friction force per length unit (l.u.)  $\mu q_z$ . Curve 2: Force per l.u. necessary for the deformation of the rubber bristles due to the velocity difference. Curve 3: Corresponds to the slip where there are no adhesion in the contact patch ( $\sigma_x^\circ$ ).

distribution is assumed to be parabolic,

$$q_z(x) = \frac{3F_z}{4a} \left( 1 - \left( \frac{x}{a} \right)^2 \right) \quad (10)$$

and the situation is as illustrated in Figure 8. Curve 1 is the maximum available friction force  $\mu q_z(x)$  according to the pressure distribution. Curve 2 is the theoretical force needed to deform the bristles due to the velocity difference  $v_{sx}$  according to (4) together with (5). The slope of this line is  $-c_p \sigma_x$ . The marked area is the total force from the resulting brush deformation. The first contact choice with only adhesion can not be achieved assuming this pressure distribution, since sliding will occur somewhere in

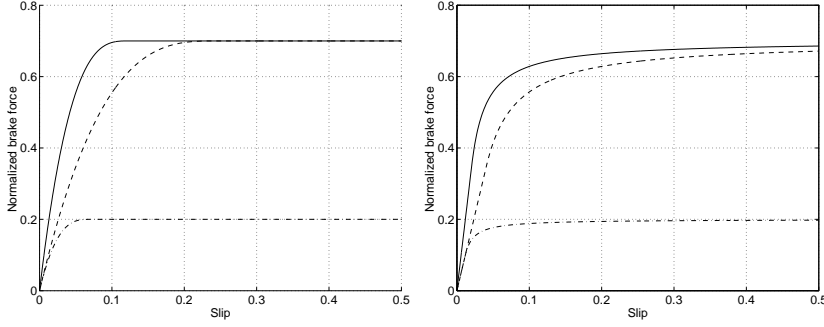


**Figure 9** Normalized brake force contra longitudinal slip ( $\sigma_x$ ) with different values of  $\mu$  and  $c_p$ . Parabolic (left) and uniform (right) pressure distribution is used in the calculations.

the region as long as the slip is nonzero. The breakaway point  $x_s$  can be derived from the following formula

$$c_p \sigma (a - x_s) = \mu q_z(x_s) \quad (11)$$

Evaluating (9) with the pressure distribution given by (10) the equation for the force-slip will be

$$F_x = 2c_p a^2 \sigma_x - \frac{4}{3} \frac{(c_p a^2 \sigma_x)^2}{\mu F_z} + \frac{8}{27} \frac{(c_p a^2 \sigma_x)^3}{(\mu F_z)^2} \quad (12)$$

According to this expression the slip behavior is mainly dependent on the tire properties at low slip. Often the relation between the force and the slip in this region is assumed to be linear with a coefficient called braking stiffness  $C_x$ . In this case  $C_x = 2c_p a^2$ . At higher slip the friction coefficient is the major source for the characteristics. If the inclination of Curve 2 in Figure 8 is steeper than the inclination of Curve 1 at  $x = a$  the entire surface will slide, which is illustrated by Curve 3. Hence, the incline of the pressure distribution at  $x = a$  sets the slip limit where the entire rubber surface starts to slide against the road. In this case it is given by

$$\sigma_{xt} = \frac{3}{2} \frac{\mu F_z}{c_p a^2} \quad (13)$$

If the slip exceeds this value the braking force will simply be put to  $F_x = \mu F_z$ .

$F_x(\sigma_x)$  is shown in Figure 9. Since constant friction is assumed the brake force is constant for slip values above  $\sigma_{xt}$ .

**Uniform pressure distribution** To show the importance of the vertical pressure distribution the calculation from above has been done assuming uniform pressure. Let  $q_z$  denote the force per length unit.

$$q_z(x) = \frac{F_z}{2a}$$

The point where sliding starts can be derived by reformulation of equation (8), hence

$$x_s = a - \frac{\mu F_z}{2c_p a \sigma}$$

For  $x_s < -a$  there is no sliding and the expression for the brake force is derived from the first integral in (9) using  $x_{cs} = a$ . In the other case the whole expression (9) is used That gives

$$F_x = \begin{cases} 2c_p a^2 \sigma & \text{if } \sigma < \mu F_z / (4c_p a^2) \\ F_z \mu - \frac{F_z^2 \mu^2}{4a^2 c_p \sigma_x} & \text{otherwise} \end{cases} \quad (14)$$

The result is shown in Figure 9. For uniform pressure we never really get the entire contact patch to slide, which can be seen on the asymptotic convergence to  $\mu$  when the slip increases.

**Lateral slip** In the lateral direction the effects of the flexibility of the carcass normally, is larger than in the longitudinal direction [13]. For better accuracy its deformation should be included in the model. The literature mainly describes two ways to handle this. The simpler one is the thread model where the carcass is treated as a thread. The more complicated is the beam model where the deformation is calculated according to the beam theory.

Deformation of the carcass according to the thread model is given by

$$S \frac{d^2 \delta_c(x)}{dx^2} = p_{cy}(x) \quad (15)$$

$S$  is the tension in the thread.  $p$  is the horizontal force per length unit. Index 'c' denotes carcass and 'b' brush. Deformation of the rubber as in the longitudinal case

$$p_{by}(x) = c_{py} \delta_b(x)$$

Total deformation of the brush in contact with the road is

$$\delta_y = \frac{v_{sy}}{v_x} x$$

The carcass and the brush element can be treated as connected serially which means that the total deformation is the sum of the two elements. The force acting on the brush is the same as the force acting on the corresponding point of carcass. This gives

$$\delta_y = \delta_c + \delta_b$$

$$p_{by} = p_{cy} = p_y$$

From this we get the following differential equation for the lateral force per length unit

$$\frac{d^2}{dx^2} \left( \frac{v_{sy}}{v_x} x - \frac{p_y(x)}{c_{py}} \right) = p_y(x)$$

Which has to be solved with the constraint that  $p_y(x)$  can not exceed  $\mu q_z$ . After having solved this equation with suitable initial conditions the total lateral force is derived by

$$F_y = \int_{-a}^a p_{ry} dx$$

If the beam model is used instead of the thread model the second derivative in equation (15) has to be exchanged for a derivative of the fourth order. The equation is rather complicated and will not be solved in this paper. A simpler approach is to assume a certain shape of the carcass deformation with an amplitude depending on the total lateral force.

**Combined slip** When there is both longitudinal and lateral slip corrections are necessary. In the case that the tire has isotropic properties (i.e. equal in all directions) the resultant of the slip vector  $(\sigma_x^2 + \sigma_y^2)^{1/2}$  can be used in the force-slip formula and the tire force acts in the opposite direction as the slip vector. A tire is, in general, not isotropic as discussed above and in [13] and [5] it is explained how the brush model can be expanded into two dimensions assuming anisotropic conditions. For empirical models, see Section 2.4, there are a lot of suggested solutions how to derive the force-slip relation for any direction of the slip vector given the results from pure lateral and pure longitudinal slip. One solution is explained in [5], which has the following important features:

- It reduces exactly to the empirical model at pure-slip.
- It gives a smooth transition from small-slip to large-slip behavior that agrees with empirical observations.
- Only few parameters are needed, which all have clear physical interpretations.
- Nominal parameter values may be derived automatically from the empirical pure-slip models.
- Differences between driving and braking conditions are accounted for.

**Discussion** This section has mainly treated the way to physically derive a relation between the braking force and the slip. The resulting expression includes the rubber stiffness  $c_p$ , the length of the contact patch  $2a$ , the tire/road friction  $\mu$ , and the vertical wheel load  $F_z$ . The vertical pressure distribution  $q_z(x)$  is another very important factor for the formula.  $c_p$  is a material parameter and is depending on the rubber thickness, i.e. it will increase when the tire wears. It is probably also depending on the temperature in the tire. In Section 2.1 there is a discussion about the relation between  $a$  and  $F_z$ . The friction is the most uncertain parameter and it is affected by factors such as road condition, slip velocity, and tread thickness. How different relations between the friction coefficient and the relative velocity affects the force-slip curve is treated in Section 4.2.

## 2.4 Empirical models

Two famous empirical models to describe the input-output formulas for a tire are presented in this section.

**Magic Formula** In [2] H. B. Pacejka presents the Magic Formula which is very well suited for describing the force-slip function as

$$F = D \sin(C \arctan(B\lambda - E(B\lambda - \arctan B\lambda))) \quad (16)$$

The parameters  $B$ ,  $C$ ,  $D$ , and  $E$  have to be identified through measurement data. Both the longitudinal and lateral force can be expressed in this

form.  $\lambda$  must, however, denote the corresponding slip according to the SAE standard, see Section 2.2. In Figure 10 the curve is plotted with parameters chosen to fit results derived from tests performed by Olle Nordstöm at VTI [11]. By changing the parameters it is possible to obtain the characteristics of other tires and road conditions.

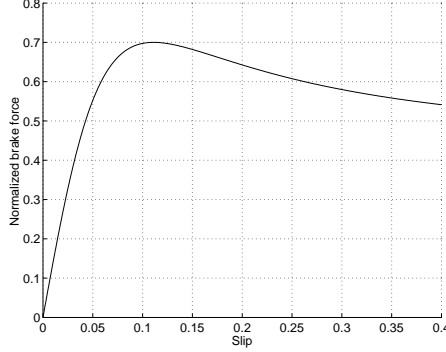


**Figure 10** Tire-road friction as a function of the slip. Curve created by the Magic Formula using the parameter values  $D=0.7$ ,  $C=2.5$ ,  $B=8$ ,  $E=1$ .

**LuGre Model** The LuGre model is well known for describing special cases of friction situations. It has been introduced in the tire modeling by C. Canudas de Wit [3] to describe the dynamic process when applying a brake torque on the tire. It also deals with the velocity dependence on the friction. It has one lumped (all forces work from one point) and one distributed approach. The lumped one is described as

$$\dot{z} = v_{sx} - \frac{\sigma_0 |v_{sx}|}{g(v_{sx})} z \quad (17a)$$

$$F_x = (\sigma_0 z + \sigma_1 \dot{z} + \sigma_2 v_{sx}) F_z \quad (17b)$$

$$g(v_{sx}) = \mu_c + (\mu_s - \mu_c) e^{-\sqrt{|v_{sx}/v_{st}|}} \quad (17c)$$

The  $z$ -state denotes the deflection of the brush elements and corresponds to  $\delta$  in Section 2.3. However, here is a dynamic relation between the slip velocity and the brush deflection. In the distributed approach,  $z$  is depending on the position in the contact patch, but in the lumped realization  $z$  denotes the average value of the deflection in the entire contact area. The lumped form has to be used for control and estimation purposes, but to be able to match the  $\sigma$ -parameters in the equations to experimental data the steady-state version of the distributed approach must be used. The procedure for this is further explained in [3] and results in the following formula

$$F_x(s) = \text{sign}(v_{sx}) F_z g(v_{sx}) \left( 1 + \left( 1 - \frac{\sigma_1 |v_{sx}|}{g(v_{sx})} \right) \frac{g(v_{sx})}{\sigma_0 2a |\lambda|} \left( e^{-\frac{\sigma_0 2a |\lambda|}{g(v_{sx})}} - 1 \right) \right) + F_z \sigma_2 v_{sx} \quad (18)$$

where  $2a$  is the length of the contact patch. There are six parameters that has to be identified in this formula. In [3] it is claimed that it can be made



look very similar to the shape of Magic Formula. In Figure 11 there is an example a force-slip curve generated by the LuGre model. This curve should not be compared to the curve in Figure 10, since the parameters for the LuGre model are not identified from that curve.

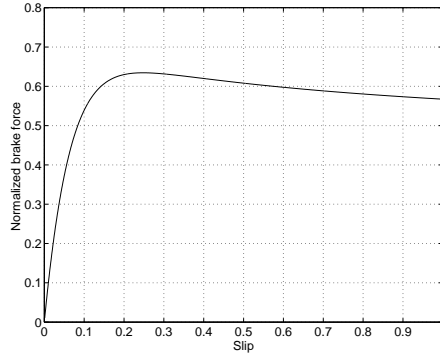


**Figure 11** Static force-slip curve generated with the LuGre-model, trying to match the Magic Formula shape

**Discussion** Two empirical models for describing the force-slip relation have been described above. Many more models are described in the literature, but after the introduction of the Magic Formula, it has become the absolutely most popular tire model. The LuGre-model is interesting while it tries to deal with the dynamics in the friction surface.

### 3. Estimation models

#### 3.1 Slip based friction estimation according to NIRA-dynamics

Estimation of the road-tire friction by examining the slip-force curve has been done by F. Gustavsson [6]. The assumption is that for low slip values the relation between the force and the slip is

$$F = ks$$

It is then stated that  $k$  is not only tire depending it is also depending on the tire-road friction  $\mu$ . By using a Kalman filter,  $k$  is estimated during driving. If a change in  $k$  is noticed the algorithm will sense it as a change in friction. The difficult part in this approach is the calibration. While  $k$  is influenced by wear and aging it is necessary to update the reference value for  $k$  when the vehicle is running on asphalt. The slip some times has an offset ( $\delta$ ), probably depending on small changes of the rolling radius of the wheel. To cover for this offset, the estimation model is

$$s = [F \ 1] \begin{bmatrix} \frac{1}{k} \\ \delta \end{bmatrix} + e(t)$$

Quick changes of  $k$  is detected by a CUMSUM detector, which temporarily increases the state noise covariance matrix in the Kalman filter, so it adapts faster to the new condition.

An important feature is that the friction estimator works together with a variance calculator. The variance of the rolling radius of the tires is calculated and it shows a significant difference between i.e. asphalt and gravel. Combining these two variables it is possible to distinguish between four different types of road surfaces, asphalt, gravel, snow, and ice. The knowledge of the  $k$  value is not enough to predict the maximum friction, but if the tire some time achieves a higher braking force better conclusions can be drawn about the friction and be remembered for the actual road condition.

The assumption that  $k$  should be dependent on  $\mu$  for low slip contradicts the theory presented in this paper and there is no physical models that supports this theory. However, according to F. Gustavsson there are experimental test done showing that there is evidence for this relationship. In any case, it seems to work well in practice and these ideas has been further developed by the company NIRA which sell a box that can be connected to the CAN-bus and then just deliver friction signals.

In [10] another approach of Gustavsson's ideas is described. The algorithm then estimates the  $k$ -value only while braking and then it is possible to use higher slip values, which would give better accuracy on the estimate. However, the method includes more uncertainties for the measurements, for example, the way of deriving the braking force from the braking pressure. So it is doubtful whether the final result is more reliable or not.

### 3.2 Brake force estimation with a Kalman-Busy Filter

In [16] a method to estimate the tire forces is described. It also covers a statistical approach to, among many tire models, choose the one that best fits the actual conditions. A vehicle model is established in state-space form.

$$\dot{x} = f(x, F, u)$$

$$y = h(x, F, u)$$

where

$$\begin{aligned} x &= [v_x \ v_y \ r \ p \ \omega_{fl} \ \omega_{fr} \ \omega_{rl} \ \omega_{rr}]^T \\ F &= [F_{xfl} \ F_{xfr} \ F_{xrl} \ F_{xrr} \ F_{yf} \ F_{yr}]^T \\ u &= [T_{fl} \ T_{fr} \ T_{rl} \ T_{rr} \ \delta]^T \\ y &= [r \ \omega_{fl} \ \omega_{fr} \ \omega_{rl} \ \omega_{rr} \ a_x \ a_y \ p]^T \end{aligned}$$

The states are the vehicle velocity, yaw, roll, and the rolling velocity of each wheel. The vector  $F$  contains the tire forces acting on the vehicle.  $u$  is the braking or accelerating torque on each wheel and the steer angle of the front wheels.  $y$  includes the states or signals that are possible to measure. From these equations the aim is to estimate the brake forces. It is done by an Extended Kalman-Busy Filter (EKBF). The states are extended to

$$x_a(t) = \begin{bmatrix} x(t) \\ F(t) \end{bmatrix} = \begin{bmatrix} f(x, F, u) \\ AF \end{bmatrix} = f_a(x_a, u)$$

$$y = h_a(x_a, u)$$

where  $A$  is a block diagonal matrix. Then it is possible to estimate the state vector  $x_a$ . While the vector includes both the vehicle velocity and wheel velocities the slip can be calculated. So it is possible to derive an relation between the normalized brake force and the slip. If a tire model is of the following form

$$F_{model} = T(\text{slip}, a, F_z, v, \mu)$$

the most probable  $\mu$  value can be calculated, by using Bayesian hypothesis selection theory, as

$$\hat{\mu}_k = \sum_{j=1}^J Pr[\mu_j | F_k] \mu_j$$

More information about the EKBF and how to calculate the  $\mu$ -probability function is given in [16]. L. R Ray refers that the algorithm has been tested in a real vehicle and the tracking of the states were good and the  $\mu$ -estimation was excellent.

### 3.3 GPS-based identification of the lateral tire-road friction coefficient

If the vehicle is equipped with a Differential Global Position System (DGPS) and a gyroscope it is possible to estimate the lateral tire friction coefficient. The following formulas can be derived from the dynamics of a vehicle:

$$\begin{aligned} m\ddot{e}_y + m\dot{\psi}_d V &= F_f + F_r \\ I_z \ddot{\psi} &= l_f F_f - l_r F_r \end{aligned}$$

where  $m$  is the mass of the vehicle and  $e_y$  is the deviation of the vehicle from the road center line. The latter is measured from the center of gravity to an interpolated line between two road coordinates. The author of the paper [7] assumes that road coordinates for all highways in America will be available in a few years.  $\psi$  is the yaw-angle and  $\dot{\psi}_d = V/R$  is the yaw rate of the road, where  $R$  is the road curvature and  $V$  the vehicle speed.  $l$  denotes the length from the center of gravity to the front respective the rear axles and  $F$  is the sum of the front respective the rear lateral wheel forces. From these formulas one can eliminate one of the forces. Eliminating  $F_r$  gives

$$\ddot{e}_y + \dot{\psi}_d \frac{I_z}{ml_r} \ddot{\psi} = \frac{l_f + l_r}{ml_r} F_f$$

The relation between  $F_f$  contra the slip angle ( $\alpha$ ) is used for the estimation and is supposed to have the same properties as the brush model described above. In [7] it is expressed in the following way

$$F_f = \Theta \Phi = \left[ C_f \frac{C_f^2}{\mu} \frac{C_f^3}{\mu^2} \right] \cdot \left[ |\tan \alpha_f| - \frac{|\tan \alpha_f|^2}{3F_z} \frac{|\tan \alpha_f|^3}{27F_z^2} \right]^T$$

The input signals are treated by a second order filter  $(s + a)^{-2}$  where  $a$  can be chosen appropriately.  $C_f$  is the cornering stiffness prior expressed by  $2c_p a^2$ .  $\alpha_f$  is the slip angle of the front wheels calculated by

$$\alpha_f = \delta_f - \tan^{-1} \frac{\dot{e}_y - (\psi - \dot{\psi}_d) V + l_f \dot{\psi}}{V}$$

where  $\delta_f$  is the steering angle. In the estimation vector we have three parameters to estimate. However, there are only two unknown constants,  $\mu$  and  $C_f$ .

$$\Theta = \begin{bmatrix} \theta_1 & \theta_2 & \frac{\theta_2^2}{\theta_1} \end{bmatrix}$$

The adaptation laws can be found in [7]. The approach has been tested on a truck and the authors stresses that the results are very efficient. The friction coefficient seems to adapt toward a true value, but oscillates around it. It is also noticed that the reliability of the estimate depends on the excitation and the amplitude of the slip. However, it is a good algorithm to distinguish between dry and slippery roads.

### 3.4 Optimal braking and friction estimation with the LuGre model

There is research going on developing observers for the friction coefficient in the LuGre tire model. The LuGre model includes six parameters which makes it flexible, but it is hard to tune all parameters by real-time estimation. The tuning is solved in the way that all parameters are matched using the steady state version of the LuGre model as described in Section 2.4. Then, the expression  $g(v_{sx})$ , see (17a), for the friction is exchanged for  $\tilde{g}(v_{sx})$  which is defined by

$$\tilde{g}(v_{sx}) = \theta g(v_{sx})$$

An observer structure for  $\theta$ , build on Lyapunov theory is presented in [4]. The estimation scheme described there can track  $\theta$  from measurements of the wheel velocity. It is implicitly assumed that the braking torque  $u_\tau$  on the rim and the normal load  $F_z$  is known.

### 3.5 Extended Braking Stiffness (XBS)

XBS is an expression for the slope of the friction force against the slip velocity at the operational point. When the XBS=0 the maximum braking force is reached. Consider the rotational dynamic function for a wheel

$$J_w \dot{v}_w = r^2 F_x - rT + r^2 d$$

where  $r$  is the wheel radius,  $T$  is the torque from the brakes,  $d$  is a disturbance and  $v_w$  is wheel velocity (m/s). The formula can be rewritten as

$$\ddot{v}_w = -\frac{kr^2}{J_w} \dot{v}_w + w$$

Here  $k$  denotes the XBS-value and  $w = r^2 \dot{d} - r\dot{T}$ . The derivatives of the signals are discretized according to the Euler approximation and the XBS is estimated with the recursive least squares algorithm with forgetting factor. The XBS-method is most powerful when one wants to control the brake around the maximal brake force point. The control law for this is further presented in [12]. It is also possible to estimate the friction coefficient from the brush model formula by using the XBS-value.

### 3.6 Lateral friction estimation using the brush tire model

In [14] the lateral tire force and the self-aligning torque are used to estimate a value of the friction coefficient. In the paper the formulas for how the torque and the lateral force depends on the slip according to the brush tire model first are derived, see also [13]. They are

$$\begin{aligned} F_y &= \frac{F_z \sigma}{\mu^2} (3\mu^2 - 3\mu\sigma + \sigma^2) \text{sign}(\alpha) \\ -M_z &= \frac{F_z a \sigma}{\mu^3} (\mu - \sigma)^3 \text{sign}(\alpha) \\ \sigma &= \frac{2c_p a^2 |\tan \alpha|}{3F_z} \end{aligned}$$

The formula for  $F_y$  is exactly the same as the one derived in Section 2.3, though it is written differently. It is then possible to get a relation between the force and the torque which is a nonlinear function depending on, for example, factors as the friction. If this relation is shown in a so called Gough plot it will look as in Figure 12. Since it can be hard to estimate something from a nonlinear relation the authors of [14] has developed a neural network with the input layer consisting of  $F_y/F_z$  and  $M_z/F_z$  and the output layer  $\alpha$  (lateral slip) and  $\mu_u$  (the utilized friction defined as  $F_y/\mu F_z$ ). The main advantage is then that one does not need to know the slip for the estimation. The higher value of the utilized friction coefficient in the examined data the better estimation precision.

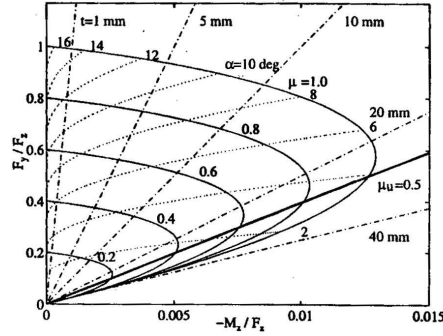


**Figure 12** Gough-plot with the normalized self aligning torque  $-M_z/F_z$  on the x-axis and the normalized lateral tire force  $F_y/F_z$  on the y-axis. Reprinted from [14].

### 3.7 Longitudinal friction estimation using the brush tire model

In [18] S. Yamazaki describes a way to estimate the longitudinal friction coefficient in real time. He formulates the brush model as

$$9\mu_x^2 F_z^2 (F_x - C_s \kappa_x) + 3\mu_x F_z C_s^2 \kappa_x^2 - \frac{C_s^3 \kappa_x^3}{3} = 0 \quad \text{if } \kappa_x < \frac{3\mu_x F_z}{C_s} \quad (19)$$

$$\mu_x = \frac{F_x}{F_z} \quad \text{otherwise} \quad (20)$$

where  $C_s$  is the the braking stiffness corresponding to  $c_p a^2$ . We can see that (19) is a reformulation of (12), however,  $\sigma_x$  is exchanged for  $\kappa_x$ . It is

not clear from the article how the estimation is performed. S. Yamazaki just claims that the friction coefficient can be easily obtained by solving (19). Measurements at two different surface conditions are performed in a drum type test machine. The measurement procedure started by having the drum and the test tire running at the same speed. Then a braking torque was slowly applied to the tire. The speed of the drum was held constant at 30 km/h. The tire will slow down and the slip velocity and the corresponding braking force are measured. For the dry surface the calculation of the friction coefficient seems to work well from 5 % slip and above. For the wet condition the calculated friction value for slips below the limit in (19) has not been closer presented.

### 3.8 Friction estimation for vehicle path prediction

Vehicle path prediction is a method to either optimize the steering and braking input to the vehicle for keeping a certain path or, at a fixed steering input, calculating when or if the vehicle will cross the outer borders of the path[9]. For these calculations an accurate tire model is necessary. When a tire develops a lateral force its longitudinal characteristics changes and the brush model given in Section 2.3 is no longer valid. C. Liu and H. Peng make the following simple extension of the brush model to take slip in two dimensions into account:

$$F_{x,y} = -\frac{k_{x,y}\sigma_x}{\sqrt{(k_x\sigma_x)^2 + (k_y\sigma_y)^2}} \left( 3c\sigma - 3\frac{1}{\mu} \frac{(c\sigma)^2}{F_z} + \frac{1}{\mu} \frac{(c\sigma)^3}{F_z^2} \right) \quad (21)$$

where  $\sigma = \sqrt{\sigma_x^2 + \sigma_y^2}$  and  $c, k_x, k_y$  are constants that relate to the tire stiffnesses. The friction coefficient can then be calculated from the brake force and the slip, even though the tire is in a combined slip situation. Two estimators to calculate the longitudinal force from the wheel speed and the torque signals are proposed. One built on the recursive least squares method and one is an enhanced adaptive observer. The bicycle model is used for the path prediction

$$\begin{aligned} \frac{d}{dt} \begin{bmatrix} y \\ \dot{y} \\ \phi - \phi_d \\ r \end{bmatrix} &= \begin{bmatrix} 0 & 1 & 0 & 0 \\ 0 & 2\frac{C_f+C_r}{mu} & -2\frac{C_f+C_r}{mu} & 2\frac{C_f a+C_r b}{mu} \\ 0 & 0 & 0 & 1 \\ 0 & 2\frac{C_f a+C_r b}{mu} & -2\frac{C_f a+C_r b}{mu} & 2\frac{C_f a^2+C_r b^2}{mu} \end{bmatrix} \begin{bmatrix} y \\ \dot{y} \\ \phi - \phi_d \\ r \end{bmatrix} \\ &+ \begin{bmatrix} 0 \\ -2\frac{C_f}{m} \\ 0 \\ -2\frac{C_f a}{I_z} \end{bmatrix} \delta_f + \begin{bmatrix} 0 \\ -u \\ -1 \\ 0 \end{bmatrix} r_d \quad (22) \end{aligned}$$

where  $r, \phi, \phi_d, y, v$  denote the yaw rate, the heading angle, the road heading angle, lateral displacement, and lateral velocity. From that the time to lane crossing (TLC) can be predicted. The predicted path is continuously compared to the real path to improve the values of the braking and cornering stiffnesses,  $C_f$  and  $C_r$ . In the model the lateral tire force is simplified to a linear function of the side slip. This will make the model only accurate at low lateral slip conditions and no longitudinal slip. The proposed

model predict a vehicle path at low slip conditions, but can also estimate the friction coefficient at combined slip, so that a warning can be issued if the force at any tire is close to exceed its maximum limit.

### 3.9 Discussion

The general way to estimate the friction coefficient includes mainly two steps. The first is to estimate the force working between the tire and the road. The second is to have a model of the tire friction from which it is possible to estimate  $\mu$  when necessary signals are given.

There are mainly two systems from where the tire forces can be estimated or measured.

- The wheel. It has fast dynamic (high bandwidth) and is situated very close to the force generation point. The tire developers works with different ways to measure the strain in the tire and from that derive the forces. There also exists equipment for torque measurement on the rim, but then the inertia of the wheel must be considered and known. Finding out the tire forces from the wheel would be most accurate method.
- The vehicle. It has slow dynamics and the connection to the force generation point is elastic.

Some of the friction estimation methods above need a good slip-signal. That could be a problem while the wheel speed for each wheel and the velocity of the vehicle have to be known. All noise and bias on the wheel sensor signal are strongly amplified in the slip calculation. The quicker filter the more necessary it is to have good measurements.

## 4. Changes to the Brush Tire Model to Enhance Friction Estimation

As seen in Section 3 the brush tire model presented in Section 2.3 is widely used to estimate the friction coefficient between the tire and the road. It is possible to derive the friction both from lateral and longitudinal pure force and slip measurements. See for example Section 3.6 and 3.8. However, for the lateral estimation case some kind of compensation for the flexible carcass has to be made, but no solution for that has been found in the literature. There are mainly two parameters that decide the shape of the force-slip curve generated by the brush tire method. First the tire brake/cornering stiffness  $2c_p a^2$  and then the maximal friction force  $\mu F_z$ .  $c_p$  is the rubber shear stiffness per length unit which varies with, for example, the tire wear.  $2a$  is the length of the contact patch between the tire and the ground, which depend mostly on the vertical load on the axle, as discussed in Section 2.1. The friction coefficient  $\mu$  can vary fast if the vehicle suddenly crosses a patch of ice or runs into a different road foundation. The vertical force  $F_z$  on each wheel can also vary quickly according to the unevenness of the road.  $F_z$  will also depend on the actions of the vehicle, since the inertia forces from its movement are brought up by the wheels. The difference between  $F_z$  and the other parameters mentioned above is that  $F_z$  is assumed to be measured and then can be treated as a known

constant in the estimation. However, the noise from the unevenness of the road shape has to be reduced by a filter.

The advantage of the brush model is its simplicity. By knowing only the two parameters, the slip characteristic up to the peak of the brake force can be determined. As noted in Section 6 some approximations have been done when deriving this simple expression. Therefore, it is of particular interest to see how its behavior agrees with the characteristics of a real tire. In Figure 13 the brush model is compared to a Magic Formula estimation from real measurement data. Both the longitudinal and lateral cases are shown. Further on only the longitudinal direction is considered, but the lateral force/slip relation is shown to illustrate the misfit due to the flexibility in the carcass. The slip on the  $x$ -axis is the SAE standard definition  $\kappa_x$  defined by  $(v_x - \Omega R_e)/v_x$  and since the input for the brush model is  $\sigma_x = (v_x - \Omega R_e)/\Omega R_e$ , rescaling has been done according to  $\sigma_x = \kappa_x/(1 - \kappa_x)$ . The longitudinal curves agree well to each other, but it is necessary to consider that the measurement has been done on a test bench and the Magic Formula approximation might not exactly cover the true characteristics. These circumstances could make the fit of the brush model to the reality both better or worse, probably worse. An estimation of the friction  $\mu$  at low slip will give a much better estimate if the curve shape is good at slip value where the effect of the second order term starts to be noticeable. A way to compensate the shape of the brush model in this area and make it more flexible could be useful and a way to calibrate the  $\mu$  estimation. In this section two physically different ways to make the brush tire formula more flexible are examined. One approach is to vary the vertical pressure distribution, another is to assume a velocity dependent friction coefficient. The aim is to introduce an extra calibration parameter for the brush tire formula.

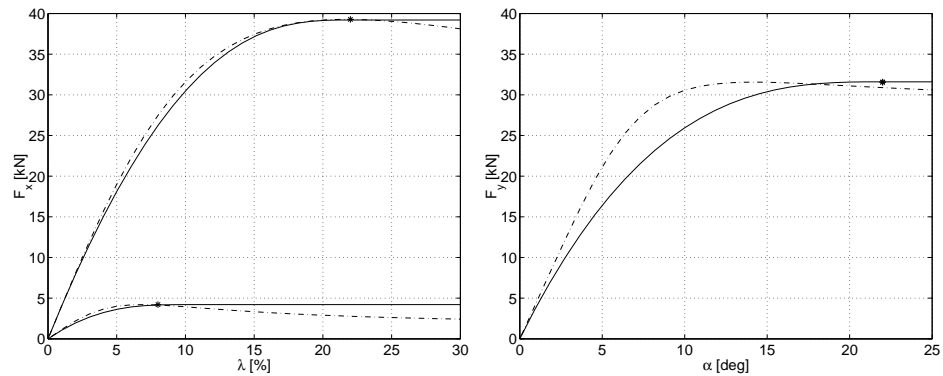


**Figure 13** Comparison of brush tire model (solid line) and a Magic Formula estimation from measurement data (dashed line). To the right is the longitudinal characteristics and the different sets of curves are from road foundations with different friction. To the left is the lateral characteristics. The difference in fit is explained by the influence of the lateral flexibility of the carcass.

#### 4.1 Pressure distribution

The brush tire model described in Section 2.3 uses parabolic pressure distribution between the tire and the road. In this chapter two different distributions are introduced and their effect on the force-slip relation is examined.



The first proposal is an asymmetric third order approach with an extra parameter which moves the top of the curve and changes the asymmetric properties. The second curve is symmetric and defined by a fourth order formulation. All equations are scaled so that the resulting force will be equal to  $F_z$ . The distributions are only defined in the longitudinal direction and supposed to be the average value of the distribution in the lateral direction. The parabolic pressure distribution used in Section 2.3 is given by

$$q_1(x) = \frac{3F_z}{4a} \left(1 - \frac{x^2}{a^2}\right) \quad (23)$$

and the asymmetric distribution is

$$q_2(x) = \frac{3F_z}{4a} \left(1 - \left(\frac{x}{a}\right)^2\right) \left(1 + d \frac{x}{a}\right) \quad (24)$$

The expression for the symmetric fourth order pressure curve is

$$q_3(x) = \frac{5F_z}{8a} \left(1 - \frac{x^4}{a^4}\right) \quad (25)$$

The curves are visualized in Figure 14. In (24) it is possible to move the point of the maximal pressure to the left or to the right by changing  $d$ . To avoid negative pressure values inside the contact patch the parameter must stay in the range of  $|d| < 1$ . A discussion about the shape of the contact patch and the pressure distribution is performed in Section 2.1 and the special case with a circular patch as to the left in Figure 2 with a very small transition region the lumped pressure distribution would have an elliptic shape ( $q_z = k_0 \sqrt{1 - (x/a)^2}$ ). Allowing a larger transition region the curve close to  $x = \pm a$  will decrease. Probably,  $q_1(x)$  then is a realistic assumption. For the second case in Section 2.1, where the contact patch is more rectangular,  $q_3(x)$  is a better choice. For these static cases the vertical pressure may not exceed the tire pressure. When the wheel rolls the continuous deformation of the tire changes the pressure distribution. The damping together with the mass forces increases the pressure at the leading side and decrease it on the trailing side. There might also be some effects from the centrifugal forces caused by the wheel rotation. The asymmetric third order function,  $q_2(x)$ , with a positive  $d$  is then a realistic choice. When a brake force is applied the carcass is strained in the leading end and compressed in the trailing end. This could have the effect of moving the center of the pressure distribution backwards and the  $d$  could then reach a negative value. A correct choice of pressure distribution needs a lot of further investigation and measurements. Later on we will see how different distributions affect the force-slip curve and that the choice of it might not be done on theoretical foundations.

**Force-slip function for an asymmetric pressure distribution.** Curve 1 in Figure 8 is now replaced by (24) and by eliminating the root  $x_s = a$  from (11) the breakaway point can be derived by

$$\frac{3 F_z \mu}{4 a^2} \left(1 + \frac{x}{a}\right) \left(1 + d \frac{x}{a}\right) = c_p \sigma_x \quad (26)$$

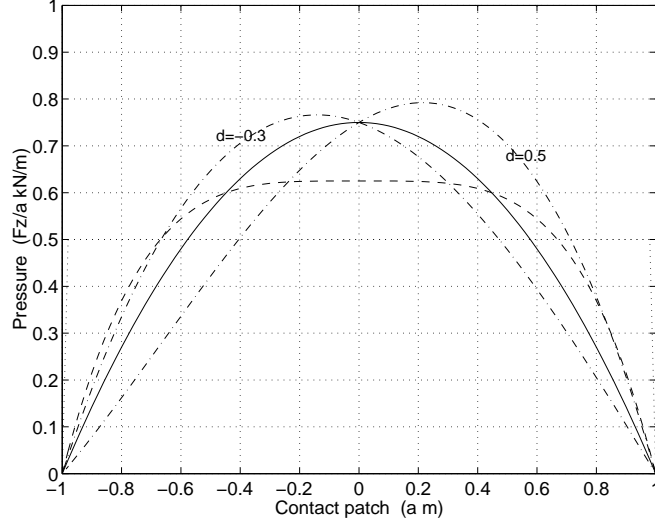


**Figure 14** The pressure distributions proposed in this chapter. The wheel is supposed to move to the right. The leading side will then be to the right and the trailing side is accordingly to the left. the solid line shows pressure distribution according to equation (23), dashed line according to equation (25) and the dashed dotted ones to equation (24) with different choices on  $d$ .

with the solutions

$$x_s = -\frac{a}{2d}(d+1) \pm \frac{a}{2d} \sqrt{(d-1)^2 + \frac{16a^2 c_p d}{3\mu F_z} \sigma_x} \quad (27)$$

To be able to use the calculation scheme from Section 2.3, one and only one solution can be inside the contact region. Therefore the sign in front of the square root has to be positive. For  $d$  less than  $-0.5$  there are two solutions inside the interval. Physically it means that there are two sliding areas split by one adhesive region. To avoid that, the interval for  $d$  is restricted to  $[-0.5, 1]$ . The total brake force, which is illustrated by the marked area in Figure 8, is described by the integral

$$F_x = \int_{-a}^{x_s} \frac{3\mu F_z}{4a} \left(1 - \left(\frac{x}{a}\right)^2\right) \left(1 + d \frac{x}{a}\right) dx + \int_{x_s}^a (a-x) c_p \sigma_x dx \quad (28)$$

which gives the following expression

$$F_x = \frac{\mu F_z}{32d^3} (1-d)^3 (3d+1) + \frac{c_p a^2}{4d^2} (2d+5d^2+1) \sigma_x + \frac{1}{3} \frac{c_p^2 a^4 \sigma_x^2}{\mu F_z d} - \left( \frac{\mu F_z}{32d^3} (d-1)^2 + \frac{c_p a^2}{6d^2} \right) (3d+1) \sigma_x \cdot \sqrt{(d-1)^2 + \frac{16d c_p \sigma_x a^2}{3\mu F_z}} \quad (29)$$

The slip limit where the entire contact area slides towards the ground is given by the incline of the pressure curve in  $x = a$ . Hence,

$$F_x = \mu F_z \quad \text{if} \quad \sigma_x > \frac{3\mu F_z}{2c_p a^2}(1 + d) \quad (30)$$

The result for some different values of  $d$  is shown in Figure 15. The complexity of (29) could be reduced by choosing  $d$  to 1 or  $-1/3$ . However, the idea to change the pressure distribution in this way is to get a calibration parameter that can be changed continuously.

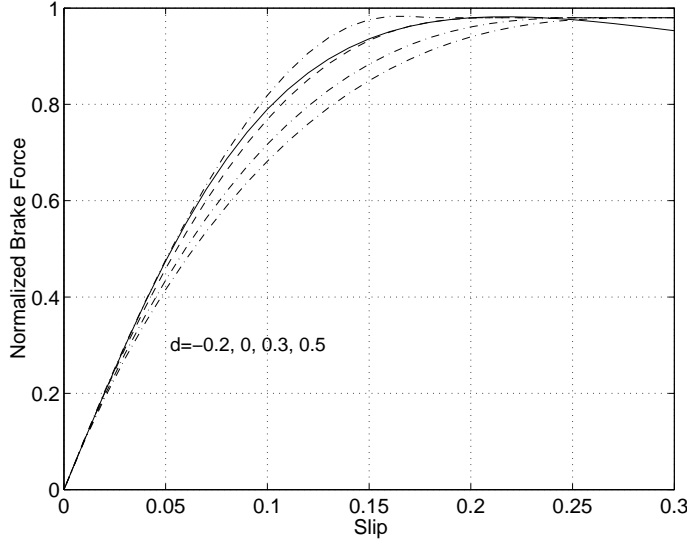


**Figure 15** Illustration showing the brake force contra the slip using the pressure distribution given by (24). The solid line denotes a Magic Formula realization from a real tire. The others are derived using different value of  $d$ .

**Symmetric fourth order pressure distribution** The same procedure as above can be done for the pressure distribution described by (25). There is no extra parameter introduced in this approach and yet the expression for the solution gets too complex to be presented. The shape of the resulting force-slip curve, which is shown in Figure 16, shows the difference using the fourth order distribution.

**Discussion** The results from the alternative brush models have so far only been compared to one Magic Formula estimation. The Magic Formula has got a lot of acceptance and is the best way to approximate measurement data by an expression. However, it might not be the entire truth. Therefore, it could be dangerous to draw too many conclusions just from this reference curve. There are also other factors than the pressure distribution that can affect the shape of the curve. Having that in mind we say that the fourth order curve matches very well at slip up to 70% of the maximal brake force. This means that the distribution is realistic at the trailing side, but the pressure should decrease faster when reaching the leading end. The parabolic pressure distribution give a good overall fit to the Magic Formula approximation. However, choosing the asymmetric curve with a

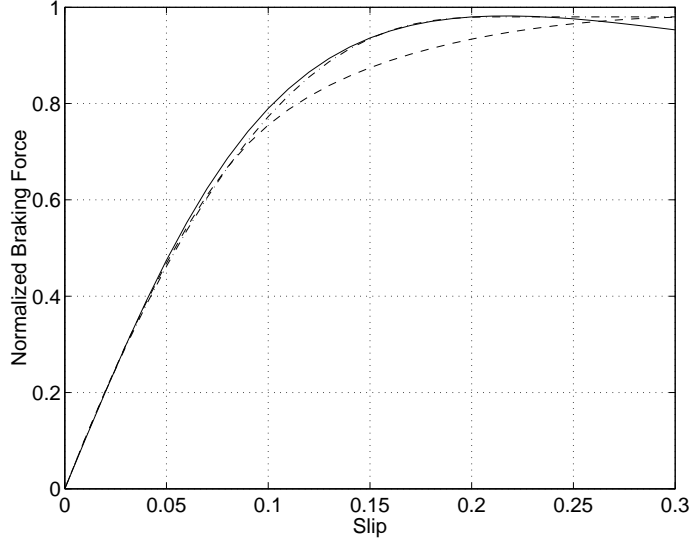


**Figure 16** Brake force contra slip. The solid line denotes a Magic Formula optimized from real data. The dashed line is derived from the fourth order pressure distribution and the dashed-dotted from the non-compensated brush model derived in Section 2.3.

slightly negative  $d$  gives better accuracy for slip up to 0.07, even though it has some mismatch at higher brake forces. That implies that the top of the pressure distribution should be a little bit behind the center of the contact patch. It could also imply that  $d$  and the peak moves with the achieved brake force, which is reasonable. Then the  $d$ -value should be changed depending on the load and brake force.

#### 4.2 Velocity dependent friction

Another way to increase the flexibility of the brush tire model is to introduce a sliding-velocity dependent friction coefficient. The bristles in the contact patch are assumed to slide against the road with the velocity  $v_{sx} = v_x \sigma_x / (\sigma_x + 1)$  directly after passing the breakaway point  $x_s$ , see Figure 8.

Three different cases of velocity dependence are treated in the following. First, in the meaning that the friction is constant but has different value whether the bristles are gripping or sliding on the road. The value  $\mu_s$  denotes the static friction and  $\mu_k$ , the kinetic. In the second case the friction coefficient is linearly dependent on the sliding velocity. Finally, an exponential relation between the friction and the sliding velocity is assumed. The two last cases are examined in two ways. Either, only the kinetic friction will be velocity dependent and the static coefficient constant or both the static and the kinetic friction have the same velocity dependence.

**Constant friction** The friction is in this case assumed to be constant, but having different values whether the bristles are sliding or gripping the road. Referring back to Section 2.3 and solving Equation (8) gives the point in the contact patch where sliding starts as

$$x_s = \frac{1}{3} \frac{\alpha (4 c_p \sigma_x a^2 - 3 \mu_s F_z)}{\mu_s F_z}$$

Evaluating (9) where  $\mu$  is changed to  $\mu_k$  gives

$$F_x = 2 c_p a^2 \sigma_x + \frac{4 c_p^2 a^4 (\mu_k - 2 \mu_s) \sigma_x^2}{3 F_z \mu_s^2} + \frac{8 c_p^3 a^6 (3 \mu_s - 2 \mu_k) \sigma_x^3}{27 F_z^2 \mu_s^3} \quad (31)$$

For  $\sigma_x > 3 \mu_s F_z / (2 c_p a^2)$  the entire surface slides and the brake force is given by

$$F_x = \mu_k F_z$$

A difference between this realization and the one from Section 2.3 is that the top of brake force curve is reached for a lower slip than total sliding occurs. By differentiating (31) and locating the zeros the slip value that corresponds to the peak force can be derived. Since (31) is a third order equation two zeros are obtained. One belonging to the maximal force and one belonging to the slip where the total sliding starts, the same point as mentioned above. The slip, where the force has its maximum, is given by

$$\sigma = \frac{3 \mu_s^2 F_z}{2 c_p a^2 (3 \mu_s - 2 \mu_k)} \quad (32)$$

and the peak force is

$$F_{max} = \frac{(4 \mu_s - 3 \mu_k) \mu_s^2}{(3 \mu_s - 2 \mu_k)^2} F_z \quad (33)$$

The calibration factor  $m$  is introduced such that the shape of the force/slip curve can be adjusted for given braking stiffness and peak brake force. Define  $m = \mu_k / \mu_s$  and the static friction can be expressed by  $\mu_s = F_{max} (3 - 2m)^2 / (F_z (4 - 3m))$  for  $m \in [0, 1]$ . In Figure 17 the force-slip curve is plotted for some different values of  $m$ . The expression for the force including the parameter  $m$  and  $\mu' = F_{max} / F_z$ , for  $\sigma_x \leq 3 \mu_s / (2 c_p a^2)$  is

$$F_x = 2 c_p a^2 \sigma_x + \frac{4 c_p^2 a^4 (m - 2) (4 - 3m)}{3 F_z \mu'} \sigma_x^2 + \frac{8 c_p^3 a^6 (4 - 3m)^2}{27 (F_z \mu')^2 (3 - 2m)^3} \sigma_x^3 \quad (34)$$

**Linear velocity dependency** To include velocity dependence on the friction, any relation  $\mu_k = f_k(v_s)$  and  $\mu_s = f_s(v_s)$  can be put into (31).  $\mu = f(v_s)$  can be put into (12) if both friction coefficients are assumed to depend on the slip velocity in the same way. Recall that  $v_s$  is the relative velocity between the tire carcass and the road. The entire sliding part in the contact patch is assumed to slide with  $v_s$ . Since the work is restricted to only longitudinal movements  $v_s = v_{sx}$  and the velocity of the vehicle  $v = v_x$ .  $v_{sx}$  can be expressed as  $\kappa_x v_x$  according to the table in Section 2.2. The expressions have to be dependent on  $\sigma_x$  instead of  $\kappa_x$  so the following transform  $v_{sx} = v_x \sigma_x / (1 + \sigma_x)$  is done. With constant static friction the following expression is used for the kinetic friction.

$$\mu_k(\sigma_x, v) = \mu_0 - n v \frac{\sigma_x}{1 + \sigma_x} \quad (35)$$

In Figure 18 the brush model characteristics is shown assuming this linear velocity dependency on only  $\mu_k$  and both  $\mu_k$  and  $\mu_s$  for two different values on  $n$ . As can be seen in the figure there is hardly any difference between using velocity dependence on the static friction or not.

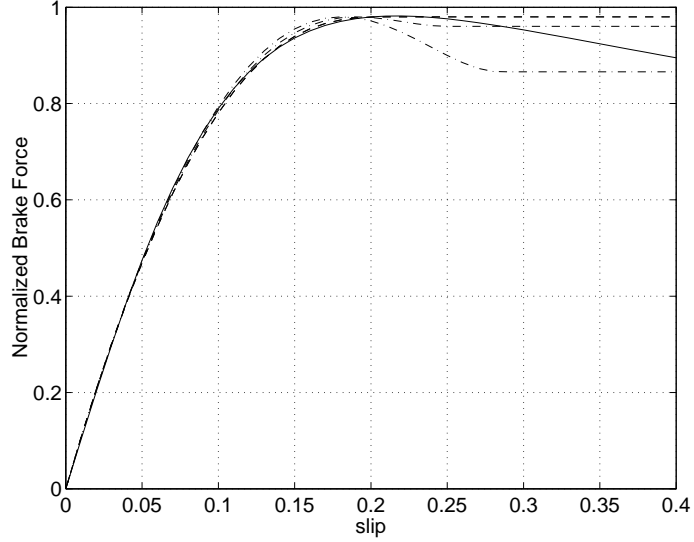


**Figure 17** The figure shows the force-slip curve derived by the brush tire model with different friction value for adhesive and sliding areas. Solid line is the Magic Formula estimated from real data. Dashed dotted curve has  $m = 1$  and dashed dotted lines has  $m$  equal to 0.6 and 0.8.

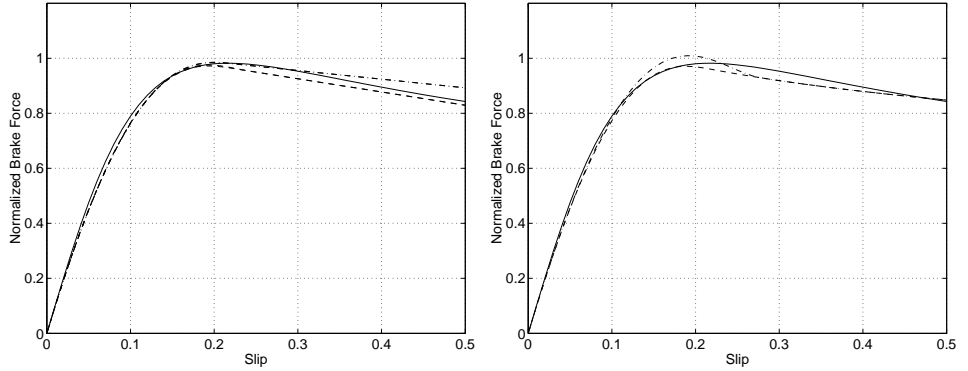


**Figure 18** The left figure shows the force-slip relation with linear velocity dependence. Solid line is the magic formula estimated from real data. The dashed curve has  $\mu_0 = 1.05$  and  $n = 0.0075$  and the dashed dotted curve has  $\mu_0 = 1.05$  and  $n = 0.0075$ . Both the case with  $\mu_s = \mu_0$  and  $\mu_s = \mu_k$  is plot, but the difference is hardly noticeable. To the right exponential velocity dependence is plotted for  $\mu = 1.3$  and  $h = 0.4$ . For the dashed dotted line  $\mu_s = \mu_0 = \mu_k(0)$  and the dashed  $\mu_s = \mu_k(v_s)$ ,

**Exponential velocity dependency** For exponential velocity dependence the following relation, which also is proposed by C. Canudas de Wit in [4], is used

$$\mu_k(\sigma_x, v) = \mu_c + (\mu_s - \mu_c) e^{-|v\sigma_x / ((1 + \sigma_x)v_{st})|^\varepsilon} \quad (36)$$

Four parameters are necessary to describe this relation. It gives good flexibility and the brush model can almost be adjusted to fit any Magic Formula set. Clearly, the aim to introduce one calibration parameter is then not fulfilled and the number of parameters has to be reduced. The reduction can be done by fixing some of parameter values. In Figure 18  $\varepsilon = 0.5$  and

$v_{st} = 30$  m/s and the calibration parameter  $h$  is introduced as

$$\mu_k(\sigma_x, v) = \mu \left( h + (1 - h) e^{-|v\sigma_x / ((1 + \sigma_x)30)|^{0.5}} \right) \quad (37)$$

The right illustration in Figure 18 shows that the difference between the adhesive and the sliding friction gives a sharp hook on the force slip curve just before entering the slip for total sliding. When studying raw data from tests of tires this phenomenon is often observed, but it is not really covered by the Magic Formula parameterization.

**Discussion** From the result in this section it can be seen that it is only possible to change the slope of the brush tire model curve at slip values close to or above the point for total sliding when using velocity dependence for calibration. This is obvious considering the fact the larger slip the larger share of the brake force is depending on the friction characteristic.

In the literature it has been shown that even the adhesive friction coefficient can be depending on the speed that pulls the materials away from its original position. Assuming the case with different static and kinetic friction gives too negative slope behind the maximal force point. This could maybe be changed by a combination of velocity dependent friction and another pressure distribution than the parabolic one. The great advantage if one could get these approximation more realistic is that it would be possible to prescribe the negative slope without or just before entering that zone.

### 4.3 Taylor expansion

Estimation of parameters using schemes as the least squares method are facilitated by use of a simple expression. Therefore, a polynomial approximation for the expression above with parameters depending on  $d$ ,  $m$ ,  $n$ , or  $h$  is performed. In this section the expressions are simplified by Taylor expansion.

**Taylor expansion of the expression for the asymmetric pressure distribution** Expanding (29) in a Taylor series, with  $d$  in the interval  $-0.5 < d < 1$ , gives the following expression:

$$\begin{aligned} F_x = & 2 c_p a^2 \sigma_x + \frac{4}{3} \frac{c_p^2 a^4}{(d-1) \mu F_z} \sigma_x^2 - \frac{8}{27} \frac{(3d+1) c_p^3 a^6}{(d-1)^3 \mu^2 F_z^2} \sigma_x^3 \\ & + \frac{16}{27} \frac{(3d+1) c_p^4 a^8 d}{(d-1)^5 F_z^3 u^3} \sigma_x^4 - \frac{128}{81} \frac{(3d+1) c_p^5 a^{10} d^2}{(d-1)^7 F_z^4 u^4} \sigma_x^5 + O(\sigma_x^6) \quad (38) \end{aligned}$$

When truncating a series expansion there is always a question about the convergence. In this case it is no restriction to a certain number of terms, but the advantage of the Taylor expansion gets lost if the convergence is slow. If  $d = -1/3$  and  $0$ , only 2 respectively 3 terms are needed to deliver exact convergence. For  $d < 0.1$  sufficient accuracy is reached using four terms. At this point ‘‘sufficient accuracy’’ is somewhat diffuse. The estimation scheme has to be set before a distinct demand on the accuracy can be determined. For higher values it is more critical and more terms are needed. Of course the convergence also depends on the value of  $c_p a^2 / \mu F_z$ . The correct expression together with Taylor expansion truncated after the three respective four terms are shown in Figure 19.

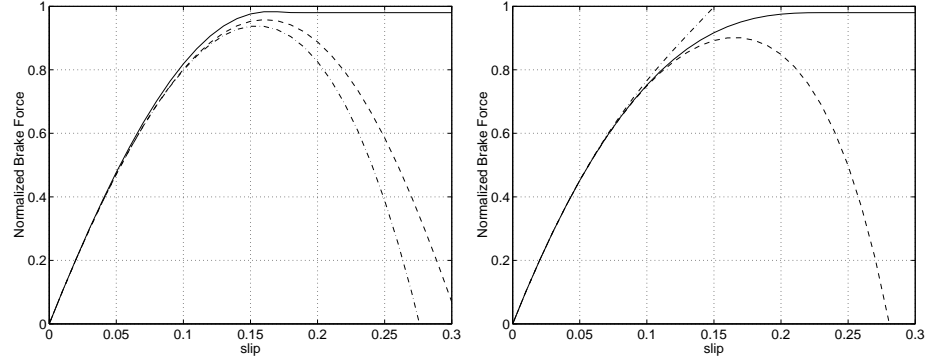


**Figure 19** Convergence of Taylor expanded brush model formula with asymmetric pressure distribution. In the left figure  $d = -0.2$  and in the right figure  $d = 0.1$ . The dashed dotted line: three terms used. The dashed line: four terms used.

#### 4.4 Velocity dependency

The Taylor expansion of linear velocity dependency up to order 4.

$$2c_p a^2 \sigma_x - \frac{4 c_p^2 a^4}{3 F_z \mu_0} \sigma_x^2 + \frac{4 c_p^2 a^4}{3 F_z \mu_0} \left( \frac{2 c_p a^2}{9 F_z \mu_0} - \frac{nv}{\mu_0} \right) \sigma_x^3 + \frac{4 c_p^2 a^4}{3 F_z \mu_0} nv \left( \frac{4 c_p a^2}{9 F_z \mu_0^2} + \frac{1}{\mu_0} - \frac{nv}{\mu_0^2} \right) \sigma_x^4 + O(s^5) \quad (39)$$

Series expansion for the exponential velocity dependence is left out since

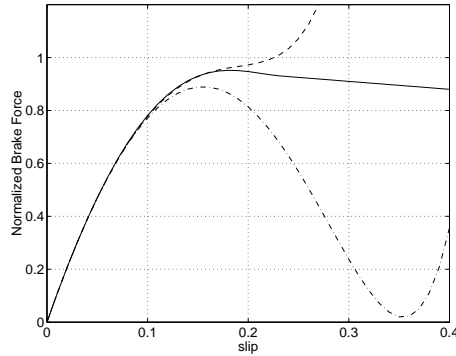


**Figure 20** Convergence of Taylor expanded brush model formula with linear velocity dependent  $\mu$ . Solid line is the correct formula. Dashed line denotes series expansion of order four and dashed dotted of order three.

it converge slowly.

**Discussion** In this section we have tried to approximate the quite complicated expressions for the modified brake force by applying series expansion. The aim is to get a simple formula that could be used for estimation, specially at low slip. For the changeable pressure distribution a good approximation using polynomials of the third order up to slip values around 0.1 can be achieved. However, the accuracy depends on the value of  $d$ , which for good result should stay within the range  $-0.4 < d < 0.1$ . The



case where the friction depends linearly with the velocity the approximation also shows a good result. for the exponential dependency it seems more difficult to approximate the derived formula by a series expansion. The convergence is not enough.

## 5. Simulation of Friction Estimation with Brush Model

The aim for the simulation in this section is to examine the possibility of estimating the friction between the tire and the road, without reaching the peak force point. The brush model explained in Section 2.3 is used, since the friction coefficient is explicitly included in the derived expression. Finally, there is a brief discussion of how different choices of the calibration factor  $d$  affects the estimates.

### 5.1 Data generation

The model for the data generation is built in Simulink and describes a wheel with a certain inertia. A torque can be applied to the wheel rim which through the tire develops a brake force. The brake force causes a velocity difference (slip) between the road and the wheel with a relation described by the Magic Formula:

$$F_x = F_z D \sin(C \arctan(B \kappa_x - E(B \kappa_x - \arctan B \kappa_x))) \quad (40)$$

where the coefficients  $B$ ,  $C$ ,  $D$ ,  $E$  have been estimated from test data. The set of coefficients used here characterize a normal tire, having a stiffness  $C_x = 5e^5$ , running on asphalt, with  $\mu = 0.98$ . On the signals necessary for the estimation noise is added with the covariances  $\sigma_\lambda^2 = 0.2 \cdot 10^{-4}$  on the slip and  $\sigma_{F_x}^2 = 0.2 \cdot 10^{-2} F_z^2$  on the force signal. Vehicle tests performed at a Scania truck have shown these values to be realistic.  $F_z$  is considered as a constant. The simulated data is generated by application of the torque in a saw tooth like manner to the wheel rim with the aim to reproduce the torque ramp that arises when the brakes are applied in a braking situation. Different amplitudes of the input signals are tested. The normalized brake force for a input signal of amplitude of 75% of the peak force is shown in Figure 21.

### 5.2 Estimation of brush model parameters

The expression for the brake force as a function of the slip using the brush tire model with the proposed calibration factor  $d$  is

$$F_x = C_x \sigma_x + \frac{1}{3} \frac{C_x^2}{(d-1) \mu F_z} \sigma_x^2 - \frac{1}{27} \frac{(3d+1) C_x^3}{\mu^2 F_z^2 (d-1)^3} \sigma_x^3 \quad (41)$$

The included coefficients are further presented in Section 2.3 and the relation between  $\sigma_x$  and  $\lambda$  is given by  $\sigma_x = \lambda/(1-\lambda)$ . The brush model can be parameterized as

$$y = \theta_0 u_0 + \theta_1 u_1 + \theta_2 u_2 + e \quad (42)$$

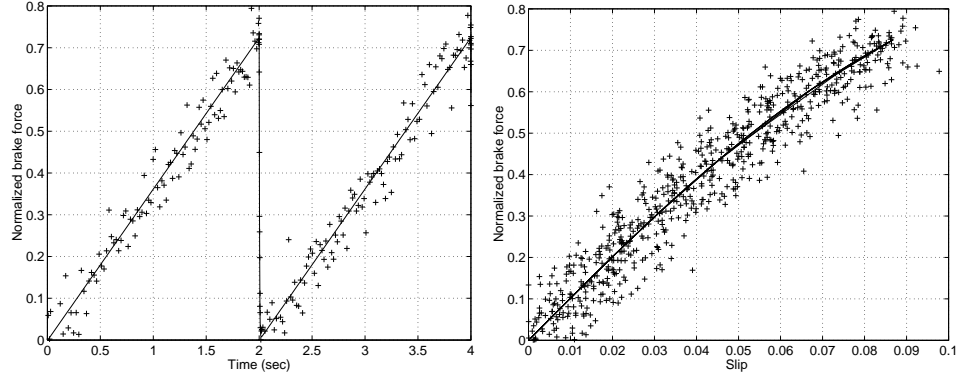


**Figure 21** To the left the input signal is shown as the normalized brake force which actually is direct proportional the input torque. To the right the same signal is shown as a function of the generated slip.

with the following regressors

$$y = \frac{F_x}{F_z} \quad (43)$$

$$u_0 = C_{x0}\sigma_x \quad (44)$$

$$u_1 = -\frac{1}{3\mu_0} \frac{(C_{x0}\sigma_x)^2}{F_z} \quad (45)$$

$$u_2 = \frac{1}{27\mu_0^2} \frac{(C_{x0}\sigma_x)^3}{F_z^2} \frac{3d+1}{(d-1)^3} = \frac{u_1^2}{3u_0} \frac{3d+1}{d-1} \quad (46)$$

The tire parameters of interest can be derived as

$$\hat{C}_x = \theta_0 C_{x0} \quad (47)$$

$$\hat{\mu} = \frac{\theta_0^2}{\theta_1} \mu_0 \quad (48)$$

Then the third parameter  $\theta_2$  can be expressed by the other two parameters  $\theta_0$  and  $\theta_1$  as  $\theta_2 = \theta_1^2/\theta_0$  and (42) can be rewritten in the following form

$$y = \theta_0 u_0 + \theta_1 u_1 + \frac{\theta_1^2}{\theta_0} \frac{u_1^2}{3u_0} \frac{3d+1}{d-1} + e \quad (49)$$

Two different estimation procedures are compared, the recursive least squares (RLS) algorithm with forgetting factor and the MIT-rule. The well-known RLS described in for example [8] works only with linear equations and the nonlinear factor has to be treated separately. Here it is included in the output signal as

$$y'(k) = y(k) - \frac{\theta_1^2(k-1)}{\theta_0(k-1)} u_2(k) \quad (50)$$

and the following linear expression,

$$y'(k) = \theta_0(k)u_0(k) + \theta_1(k)u_1(k) + e(k) \quad (51)$$

can be used for update of the  $\theta$ -parameters.

The MIT-rule [1] treats the nonlinearity and to update each parameter the formula

$$d\theta_i = -\gamma e \frac{\partial e}{\partial \theta_i} \quad (52)$$

is used and  $e$  and its partial derivatives can be derived from (49).

### 5.3 Estimation results

When deriving the results from the estimation using RLS and the MIT-rule, the calibration factor is set to zero, i.e.  $d = 0$ , which means that its influence is not present at all. The amplitude of the used input signal is either 50% or 75% of the maximal friction utilization. The normalization factors  $C_{x0}$  and  $\mu_0$  are set to 50 kN respective 0.98, so the optimal values for the estimated parameters would be unity if the brush model and the tire characteristic were identical. The variance matrix for the RLS estimation is set to  $\text{diag}(2, 10) \cdot 10^{-10}$  and the forgetting factor to 0.999. For the MIT-rule  $\gamma_0 = 0.5 \cdot 10^{-10}$  and  $\gamma_1 = 3 \cdot 10^{-10}$ . The initial condition on  $\theta$  is  $[0.8, 0.8]$ .

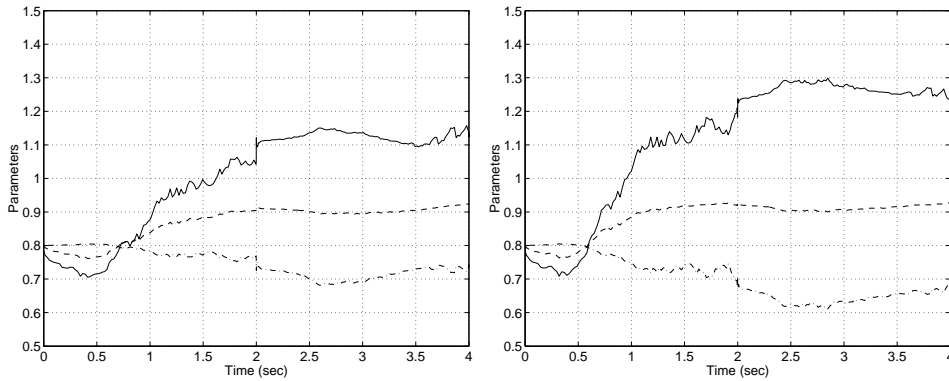


**Figure 22** Plot of results from estimation with RLS. The input signal has the amplitude of 50% of the peak force to the left and 75% of the peak force to the right. Solid line:  $\mu$ , dashed line:  $\theta_1$  and dashed dotted line:  $\theta_2$ .

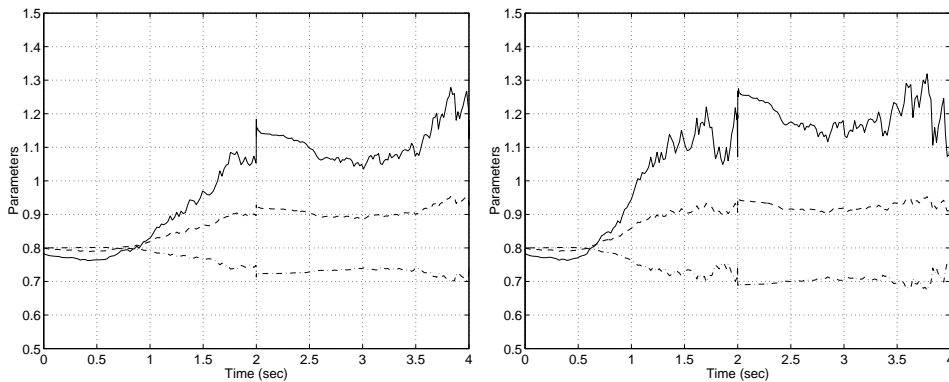


**Figure 23** Plot of results from estimation with MIT,  $d$  set to zero and with the input signal as 50% of the peak force to the left and 75% to the right.

The estimation according to RLS is shown in Figure 22 and according to the MIT-rule in Figure 23. The result seems to converge well with more

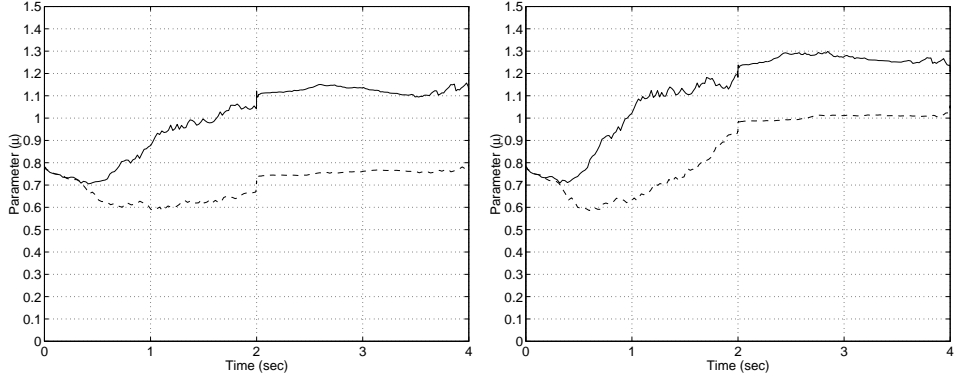


**Figure 24** Illustration of the difference between the estimation of two different tires with different friction. To the left the input signal is 50 % of the peak force for the original tire and to the right the input signal is 75 %. Solid line denotes the tire previously used the dashed line denotes the new one.

accurate estimate for the lower input signal in both cases. This was not as expected and it was found out that the initial conditions together with the update speed of  $\theta_1$  are very important for the estimation result, specially for the lower force case. In reality most often the parameters are more or less known and the initial values not need to differ much the real values, but changes has to be detected. Therefore an additional estimation was performed on an tire with less friction. The result is shown in Figure 24. Since the friction coefficient was lower the input signal now reached 56% and 85% of the brake force peak for the same amplitude that was used for the first tire. The result clearly shows that friction estimation with the brush model is possible, at least to discover changes. The bias in the final estimate hopefully can be reduced by better adjustment of updating. Also the irregularity in the estimation at the time  $t = 2$  s, when the input signal gets down to zero requires further work on the algorithm. Once again it must be pointed out that real tire data was used, but it came from laboratorial environment and implementation in reality can differ significantly. The described method to introduce calibration factors is one attempt to cover for this uncertainty.

#### 5.4 Effect of the calibrating $d$ -factor

To verify and examine the function of the calibration factor introduced in Section 4 and the accuracy of the Taylor expansion, an optimization was performed. The parameters,  $\theta_1 = c_p a^2$  and  $\theta_2 = \mu F_z$ , included in (38) were chosen to minimize the error between the brush model curve and the real tire data for forces up to 60% of the peak value and with different value on  $d$ . The optimization was done for two or three terms. In Figure 25 the results for the obtained parameter values inserted in (29) are shown. It clearly shows the difference when using two or three terms for the optimization. By using a correct calibration factor the effect of the truncation can be diminished and an accurate estimation can be achieved for few terms.

Since two terms seem to give accuracy enough for low slip, on-line friction estimation using the recursive least squares method might be performed. This has been verified by simulations, where the input signal, i.e.

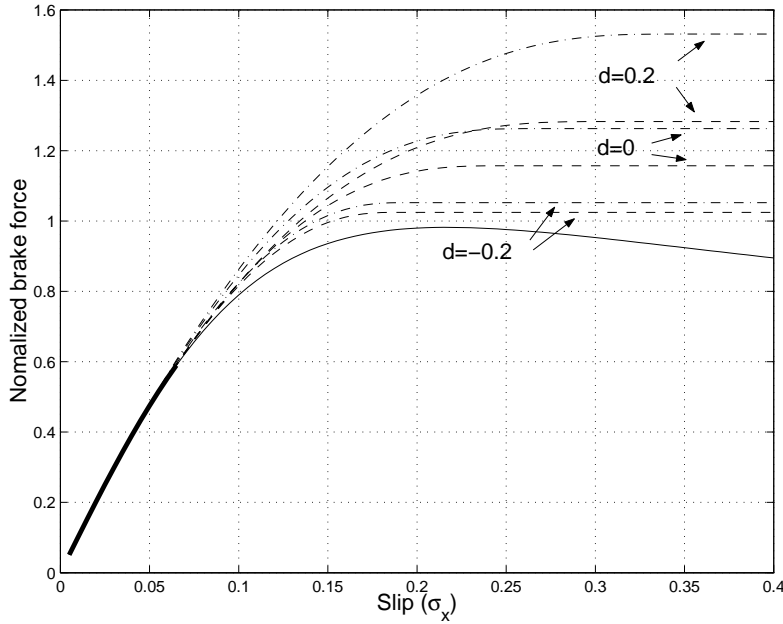


**Figure 25** Plot showing optimization of (38) to real tire data with different values of  $d$  (Dotted lines: Three terms used, dashed dotted lines: two terms used). The solid line is the Magic Formula representation and the thicker part of it specifies the optimization interval.

the brake force, is continuously applied to the tire as a repeated ramp function. The arisen slip is calculated according to the Magic Formula representation previously used in the paper. The maximum value of the input signal is 60% of the peak force value and the corresponding slip is around 4 %. The parameters,  $2c_p a^2$  and  $\mu F_z$  is estimated and the resulting  $\mu$  (assuming constant  $F_z$ ) is shown in Figure 26. The difference between the estimates is clearly visible, with a of  $d$  between  $-0.2$  and  $0$  giving the estimate best agreement to  $\mu = 0.98$ .

## 6. Conclusions

This report has given a review of tire modeling and friction estimation. The brush model has been thoroughly described and expanded by use of calibration factors, introduced in the model by inclusion of different physical properties. The parabolic pressure distribution has been replaced by a third order formula containing a parameter to modify the shape of the pressure curve. The friction coefficient has been enabled to depend on the sliding velocity, with various relations constrained by different parameters. The effect on the final force-slip relation is different depending on which of the methods that is used. Variations of the pressure distribution allows correction at slip lower than the peak force point. The velocity dependent friction mainly affects the tire model at slip values around or above the peak force depending on the choice of relation. For critical braking and ABS-situations, knowledge about the velocity dependence is useful. However, for control algorithms aiming at avoiding ABS-situations, the critical peak force is a more valuable information. This is of great concern for this

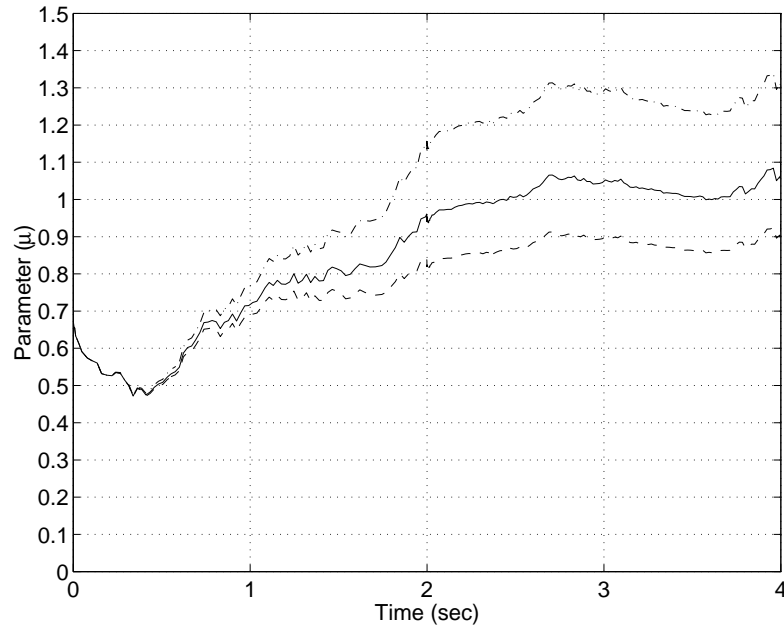


**Figure 26** Plot showing the friction estimation using the modified brush-model(38) with two terms and  $d$  equal to  $-0.2$  (dashed line),  $0$  (solid line), and  $0.2$  (dashed dotted line).

work and the model with varying pressure distribution, has been most deeply examined and tested. The modified brush models have been compared to a Magic formula approximation of real tire data, generated in laboratorial environment. According to the comparison the need of a modification in the brush model is moderate, since the curves agree well to each other. Since future implementations will be in real environment, a more realistic scenario would be to use real tire measurement data points directly in the comparison. Because the Magic Formula does not entirely cover the true tire behavior and real road conditions differ from laboratorial. The lack of data has been a restriction in the work so far, but the increased flexibility of the modified brush model is a tool to cover for uncertainties in the reality. The report concludes with a simulation of friction estimation using the brush model. This has been described in many papers, but not really seemed to be tested in reality. In the simulation environment the method can distinguish between tires with different friction. However, better estimation schemes and more work on adjusting gain-factors for the updating is necessary. A parameter optimization at the end shows that the introduction of the  $d$ -factor enhances the estimation at low slip.

## 7. References

- [1] K. J. Åström and B. Wittenmark. *Adaptiv Control*. Addison-Wesley Pub Co, 1994.
- [2] E. Bakker, H.B. Pacejka, and L. Lidner. A new tire model with an application in vehicle dynamics studies. *SAE 890087*, 1989.
- [3] Carlos Canudas de Wit and Panagiotis Tsiotras. Dynamic tire friction models for vehicle traction control. In *Proceedings of the 38th IEEE Conference on Decision and Control*, volume 4, pages 3746–3751, 1999.
- [4] Carlos Canudas de Wit, Panagiotis Tsiotras, and Xavier Claeys. Friction tire/road modeling, estimation and optimal braking control. In *Lund NACO2 Workshop*, 2001.
- [5] M. Gäfvert and J. Svendenius. Construction of semi empirical tire models for combined slip. Technical Report ISRN LUTFD2/TFRT—7606—SE, Department of Automatic Control, LTH, Sweden, May 2003.
- [6] Fredrik Gustafsson. Slip-based tire-road friction estimation. *Automatica*, 33(6):1087–1099, 1997.
- [7] Jin-Oh Hahn, Rajesh Rajamani, and Lee Alexander. Gps-based real-time identification of tire-road friction coefficient. *IEEE Transactions on Control Systems Technology*, 10(3):331–343, May 2002.
- [8] Rolf Johansson. *System Modeling and Identification*. Prentice Hall, 2002.
- [9] C.-S. Liu and H. Peng. Road friction coefficient estimation for vehicle path prediction. *Vehicle system Dynamics*, 25:413–425, 1996.
- [10] Stefan Muller and Michael Uchanski. Slip-based tire-road friction estimation during braking. In *Proceedings of IMECE01*. ASME, 2001.
- [11] Olle Nordström. *Antilås system för tungafordon, VTI Rapport nr 257*. Klintland grafiska, 1983.
- [12] Eiichi Ono, Katsuhira Asano, and Masaru Sugai. Estimation of automotive tire force characteristics using wheel velocity. In *IFAC Triennial World congress*, volume 15, 2002.
- [13] H.B. Pacejka. *Modeling of the Pneumatic Tyre and its Impact on Vehicle Dynamic Behavior*. Delft, Delft, 1988.
- [14] W. R. Pasterkamp and H. B. Pacejka. The tyre as a sensor to estimate friction. *Vehicle System Dynamics*, 27, 1997.
- [15] J.P. Pauwelussen, Gabriel Anghelache, Claudiu Theodorescu, and A. Schmeitz. *European Tire School*, chapter Module 10 - Truck tyre behavior in use and testing methods.
- [16] Laura Ray. Nonlinear tire force estimation and road friction identification: Simulation and experiments. *Automatica*, 33(10):1819–1833, 1997.
- [17] J. Y. Wong. *Theory of Ground Vehicles*. Number ISBN 0-471-35461-9. John Wiley & Sons, Inc., 2001.
- [18] S. Yamazaki, O. Furukawa, and T. Suzuki. Study on real time estimation of tire to road friction. *Vehicle System Dynamics*, 27, 1997.